

Impact of intra and inter-cluster coupling balance on the performance of nonlinear networked systems

Jiachen Ye^{1,2,3}, Peng Ji^{1,2,3*} and David Waxman^{1,2}, Wei Lin^{1,2,3}, Yamir Moreno^{4,5,6†}

¹*Institute of Science and Technology for Brain-Inspired Intelligence, Fudan University, Shanghai 200433, China*

²*LCNBI and LMNS (Fudan University), Ministry of Education, Shanghai 200433, China*

³*Research Institute of Intelligent and Complex Systems, Fudan University, Shanghai 200433, China*

⁴*Institute for Biocomputation and Physics of Complex Systems (BIFI), University of Zaragoza, 50018 Zaragoza, Spain*

⁵*Department of Theoretical Physics, University of Zaragoza, 50018 Zaragoza, Spain and*

⁶*ISI Foundation, Via Chisola 5, 10126 Torino, Italy*

(Dated:)

The dynamical and structural aspects of cluster synchronization (CS) in complex systems have been intensively investigated in recent years. Here, we study CS of dynamical systems with intra- and inter-cluster couplings. We propose new metrics that describe the performance of such systems and evaluate them as a function of the strength of the couplings within and between clusters. We obtain analytical results that indicate that spectral differences between the Laplacian matrices associated with the partition between intra- and inter-couplings directly affect the proposed metrics of system performance. Our results show that the dynamics of the system might exhibit an optimal balance that optimizes its performance. Our work provides new insights into the way specific symmetry properties relate to collective behavior, and could lead to new forms to increase the controllability of complex systems and to optimize their stability.

I. INTRODUCTION

The relationship between the structure of networks and the dynamics of the systems they represent plays a key role in a variety of collective phenomena exhibited by natural and engineered systems [1–5]. Of particular interest is the observation that in many systems patterns that correspond to synchronized clusters emerge. This phenomenon, known as *cluster synchronization* (CS), is a widespread (and characteristic) illustration of intra-cluster coherence and inter-clusters incoherence [6–9]. The understanding of the characteristics of CS is of key relevance, as it has been argued that this phenomenon is of central importance for the proper functioning of nonlinear systems that have evolved or been designed, such as the human brain [10–13] and power grids [14–17]. Despite several attempts, it is not year clear whether CS will occur and how to identify or predict in advance its emergence.

On the one hand, a considerable amount of prior work has been devoted to the issue of establishing a compact representation of the relationship between the structure and the dynamics [6, 7, 18–21] in systems that display CS. Such a representation facilitates understanding the mechanisms that eventually produce cluster synchronization. For instance, it has been observed that underlying structural symmetries can induce patterns of CS. Interestingly, the reverse is also true, namely, CS can reveal underlying symmetries [9, 20]. Patterns of CS have also been shown, both experimentally and theoretically, to be induced by modulating structures and by heterogeneous time-delayed couplings [22, 23].

On the other hand, and leaving aside the identification of numerous types of emergent CS patterns, the focus has recently been placed in studying the persistence of CS. Group theory, for example, uses the connection between symmetries and nonlinear performance measures to get new insights into the dynamical behavior of both simple [21] and arbitrarily complex networks [9]. Indeed, applying group theory to dynamically equivalent networks facilitates the detection of cluster synchronization patterns [6]. Additionally, both the degree of cluster symmetry and the spatial distribution of coupling strengths are key factors for the stability of CS. Admittedly, higher symmetries lead to a reduced region of stability [19], whereas intra-cluster couplings that are higher than inter-clusters couplings can induce stronger *local* exponential stability in networks of heterogeneous Kuramoto oscillators [7]. However, to the best of our knowledge, no prior work has investigated the *partitioning* of coupling within and between clusters, and its relation to nonlinear performance measures on realistic networks.

In this work, we are concerned with the synchronization of clusters in a general setting, as quantified by two performance metrics. We address the effects of the differences between within and between cluster couplings (henceforth

*Electronic address: pengji@fudan.edu.cn

†Electronic address: yamir.moreno@gmail.com

called the *balance* between such couplings) on two performance metrics. We use irreducible group representations to bridge the connection between structural clusters and the nonlinear performance measures, and provide a general theory that is shown to work for the Kuramoto model and an ecological model. The analytical results are consistent, to a good accuracy, with numerical simulations for several combinations of intra- and inter-cluster couplings.

II. METHODOLOGY

We consider the following classical dynamical equations

$$\dot{\mathbf{x}}_i(t) = \mathbf{F}(\mathbf{x}_i(t)) - \sum_{j=1}^N k_{ij} A_{ij} \mathbf{G}(\mathbf{x}_i(t), \mathbf{x}_j(t)), \quad i = 1, 2, \dots, N, \quad (1)$$

where \mathbf{x}_i is an n -dimensional column vector characterizing the state of the i 'th oscillator; \mathbf{F} represents the intrinsic dynamics of each oscillator; and k_{ij} quantifies the strength of the coupling between nodes i and j . Moreover, A_{ij} are the elements of a symmetric adjacency matrix $A = \{A_{ij}\}$ which encodes the connectivity pattern of the underlying network, with A_{ij} equal to 1 if oscillators i and j are connected and 0 otherwise. Finally, \mathbf{G} is the output function of adjacency oscillators, and is also an n -dimensional column vector. Eq. (1) governs the general dynamics of numerous network-coupled systems and allows, for instance, to establish a connection between network symmetries and cluster formation [9], and to capture how the rules of spatiotemporal signal-propagation depend on a network's topology [24].

As it is known, the structure of a complex system often determines many emergent behaviors and the functioning of the system. For the current phenomenon of interest, CS, the relationship structure-dynamics is no less, that is, the underlying topological features of a network play a key role in the emergence of cluster synchronization. Based on group theory, we can identify symmetries of a network with N nodes and further partition nodes into M clusters, where nodes within the same cluster have identical dynamical behavior [9]. For notational convenience, we use C_m ($m = 1, 2, \dots, M$) to denote the set of nodes in the m 'th cluster, with all nodes in C_m having identical states (i.e., identical \mathbf{x}_i) that are given by $\mathbf{s}_m(t)$ and which correspond to synchronous motion. We introduce $\alpha(i)$, within the range of $[1, M]$, which maps node i onto its corresponding cluster.

We impose small perturbations on the state of each oscillator, which corresponds to a small deviation away from the global state of M synchronized clusters. If $\delta \mathbf{x}_i$ is the perturbation of the state of the i 'th oscillator, we have $\mathbf{x}_i = \mathbf{s}_{\alpha(i)} + \delta \mathbf{x}_i$. We define $\delta \mathbf{x} = [\delta \mathbf{x}_1^T, \delta \mathbf{x}_2^T, \dots, \delta \mathbf{x}_N^T]^T$, which is an n -dimensional column vector that contains all perturbations. The corresponding linearized equation of the perturbations is

$$\delta \dot{\mathbf{x}} = [D\mathbf{F}(\mathbf{s}) - D\mathbf{G}(\mathbf{s}, \mathbf{s})] \delta \mathbf{x}, \quad (2)$$

where $D\mathbf{F}(\mathbf{s}) = \text{diag} [D\mathbf{F}(\mathbf{s}_{\alpha(1)}), D\mathbf{F}(\mathbf{s}_{\alpha(2)}), \dots, D\mathbf{F}(\mathbf{s}_{\alpha(N)})]$, $D\mathbf{F}$ is the $n \times n$ Jacobian matrix of \mathbf{F} , and $D\mathbf{G}(\mathbf{s}, \mathbf{s})$ is given by

$$D\mathbf{G}(\mathbf{s}, \mathbf{s})_{ij} = \begin{cases} \sum_{j=1}^N k_{ij} A_{ij} D\mathbf{G}_1(\mathbf{s}_{\alpha(i)}, \mathbf{s}_{\alpha(j)}), & i = j, \\ k_{ij} A_{ij} D\mathbf{G}_2(\mathbf{s}_{\alpha(i)}, \mathbf{s}_{\alpha(j)}), & i \neq j, \end{cases} \quad (3)$$

while $D\mathbf{G}_1$ and $D\mathbf{G}_2$ are, respectively, the first and last n columns of the $n \times 2n$ Jacobian matrix of \mathbf{G} .

Let us now introduce a coherency metric, H , which represents the energy expended when the system relaxes back to its stable state. In terms of a quadratic cost of phase differences between any pair of connecting nodes (following [25]), the metric H is given by

$$H = \int_0^\infty \sum_{l=1}^n \sum_{i,j=1}^N A_{ij} [\delta \mathbf{x}_i^l(t) - \delta \mathbf{x}_j^l(t)]^2 dt = 2 \sum_{l=1}^n \int_0^\infty \delta \mathbf{x}^{l^T}(t) L \delta \mathbf{x}^l(t) dt, \quad (4)$$

where $\delta \mathbf{x}_i^l$ is the l 'th component of $\delta \mathbf{x}_i$ and $\delta \mathbf{x}^l = [\delta \mathbf{x}_1^l, \delta \mathbf{x}_2^l, \dots, \delta \mathbf{x}_N^l]^T$. L is the Laplacian matrix associated with the adjacency matrix A , and it is defined as $L = D - A$ where D is the diagonal matrix whose elements are the nodes' degree.

The coherency metric, H , combines intra- and inter-clusters' interaction and separation, but this combination is hidden in the underlying structure. In order to get a deeper insight into the different contributions to H , we introduce

another performance metric, henceforth denoted by J , which is based on a simple 2 norm that captures the phase variance of the whole system. Therefore, we define

$$J = \int_0^\infty \|\delta \mathbf{x}(t)\|_2^2 dt = \int_0^\infty \delta \mathbf{x}^T(t) \delta \mathbf{x}(t) dt. \quad (5)$$

Let us now define a new coordinate system. To this end, we capitalize on some studies that have found that a unitary matrix T , which depends on A , provides a powerful way to transform the linearized equation, Eq.(2), into a convenient new coordinate system. In this new coordinate system, the transformed coupling matrix $B = TAT^{-1}$ has a block diagonal form, reflecting the symmetry structure and revealing the hidden clusters' interaction and separation [9]. Specifically, the upper-left block of B is an $M \times M$ matrix that describes the dynamics within the synchronization manifold. The remaining diagonal blocks describe motion transverse to this manifold. Applying T to Eq. (2), we rewrite this linearized equation as

$$\dot{\boldsymbol{\eta}} = \mathcal{T}[D\mathbf{F}(\mathbf{s}) - D\mathbf{G}(\mathbf{s}, \mathbf{s})]\mathcal{T}^{-1}\boldsymbol{\eta}, \quad (6)$$

where $\mathcal{T} = T \otimes I_n$ and $\boldsymbol{\eta} = \mathcal{T}\delta \mathbf{x}$. Based on the new coordinate system, Eq. (5) can be rewritten as

$$J = \int_0^\infty [\mathcal{T}\delta \mathbf{x}(t)]^T [\mathcal{T}\delta \mathbf{x}(t)] dt = \int_0^\infty \boldsymbol{\eta}^T(t) \boldsymbol{\eta}(t) dt. \quad (7)$$

Denoting the first Mn and last $(N - M)n$ exponents of $\boldsymbol{\eta}$ by $\boldsymbol{\eta}_+$ and $\boldsymbol{\eta}_-$, respectively, we divide J into

$$J_+ = \int_0^\infty \boldsymbol{\eta}_+^T(t) \boldsymbol{\eta}_+(t) dt \quad \text{and} \quad J_- = \int_0^\infty \boldsymbol{\eta}_-^T(t) \boldsymbol{\eta}_-(t) dt. \quad (8)$$

J_+ and J_- sum the intra-clusters integration and intra-clusters separation, respectively, across clusters. While J reveals more details of the hidden intra- and inter-cluster combinations, both the coherency metric H and the transformed metric J capture the system stability but from different perspectives. Note that small values of both metrics represent high levels of robustness of the system against disturbances.

Of further interest is to investigate how a redistribution of the intra- and inter-cluster coupling strengths influence the values of H and J . For simplicity, we consider the coupling strength matrix $K_{M \times M}$, where the diagonal elements represent the homogeneous intra-coupling strengths between nodes within the same cluster and the off-diagonal elements stand for the heterogeneous inter-coupling strengths between different clusters. The minimization problem (recall that the smaller the value, the higher the robustness) can be formulated as

$$\min H \quad \text{subject to } \varphi(K) = c \quad (9)$$

where $\varphi(\cdot)$ is a constraint function on elements of K and c is a constant. To address the minimization problem, we can further solve the lagrangian

$$\mathcal{L}(K, \lambda) = H - \lambda[\varphi(K_{11}, \dots, K_{MM}) - c], \quad (10)$$

and obtain the optimal solution satisfying

$$\begin{cases} \frac{\partial \mathcal{L}}{\partial K_{ij}} = \frac{\partial H}{\partial K_{ij}} - \lambda \frac{\partial \varphi}{\partial K_{ij}} = 0, & i, j = 1, 2, \dots, M, \\ \frac{\partial \mathcal{L}}{\partial \lambda} = \varphi(K) - c = 0. \end{cases} \quad (11)$$

The above procedure can also be applied to the optimization solution for minimizing J .

III. APPLICATION TO TWO PARADIGMATIC DYNAMICS

A. Kuramoto model

To further analyze the stability of the system with respect to the balance between intra- and inter-couplings, we first consider the classical Kuramoto model, which is governed by the equations

$$\dot{\theta}_i = P_i - \sum_{j=1}^N k_{ij} A_{ij} \sin(\theta_j - \theta_i), \quad i = 1, 2, \dots, N, \quad (12)$$

in which $F(\theta_i) = P_i$, and $G(\theta_i, \theta_j) = \sin(\theta_j - \theta_i)$. When the system operates within the regime of stable synchronization, we can build the corresponding Jacobian matrix and, from Eq. (3), get that $DG_1(\theta_i, \theta_j) = -\cos(\theta_j - \theta_i) \approx -1$ and $DG_2(\theta_i, \theta_j) = \cos(\theta_j - \theta_i) \approx 1$.

Regarding the coupling balance, one should (in theory) use the Lagrangian of the problem to determine all elements of the coupling-strength matrix K . Although this problem may be solvable, in general, the results obtained are hard to interpret. For simplicity, we only consider diagonal elements of K equal to k_1 (the coupling strength within clusters), and the off-diagonal elements of K equal to k_2 (the coupling strength between clusters). After an arbitrary set of disturbances, $\delta\boldsymbol{\theta}(0) = \mathbf{v}$, where $\mathbf{v} = [v_1, v_2, \dots, v_N]^T \in \mathbb{R}^N$ represents the magnitudes of the disturbances on nodes, one can obtain the explicit solution of $\delta\boldsymbol{\theta}$ from Eq. (2) as

$$\delta\boldsymbol{\theta} = e^{-(k_1 L_1 + k_2 L_2)t} \mathbf{v} = e^{-L_k t} \mathbf{v}, \quad (13)$$

where L_1 and L_2 are the intra-cluster and inter-cluster parts of the Laplacian matrix L_k , and $L_k = k_1 L_1 + k_2 L_2$. Here, $L_1 = D^{(1)} - A^{(1)}$ and $L_2 = D^{(2)} - A^{(2)}$. Specifically, $D^{(1)} = \text{diag}\{d_i^{(1)}\}$, where $d_i^{(1)}$ counts the number of intra-clusters links connecting i within the same cluster $C_{\alpha(i)}$, and $A^{(1)} = \{A_{ij}^{(1)}\}$, with $A_{ij}^{(1)}$ representing intra-clusters links between nodes i and j within $C_{\alpha(i)}$. $D^{(2)}$ is defined in the same way but for inter-cluster connections, that is, $D^{(2)} = \text{diag}\{d_i^{(2)}\}$ counts the number of inter-clusters edges linking node i to nodes that belong to different clusters, and $A^{(2)} = \{A_{ij}^{(2)}\}$ represents inter-cluster edges.

Given the explicit solution of $\delta\boldsymbol{\theta}$, we can calculate the coherency metric as

$$H = 2 \int_0^\infty \delta\boldsymbol{\theta}^T(t) L \delta\boldsymbol{\theta}(t) dt = \mathbf{v}^T \left(\sum_{i=2}^N \frac{1}{\lambda_i} u_i u_i^T \right) L \mathbf{v}, \quad (14)$$

(see S2 for the detailed calculation) where λ_i and u_i ($i = 2, 3, \dots, N$) are the eigenvalues of L_k from the smallest to the largest except for $\lambda_1 = 0$ and the corresponding eigenvectors, respectively.

We implement the constraint $k_1 + k_2 = 1$, that forces a partition of couplings, and allows the investigation of the effects of the intra and inter-coupling balance on the coherency metric H . We proceed by obtaining the first and the second derivatives of H with respect to k_1 (see S2), which leads to

$$\begin{cases} \frac{dH(k_1)}{dk_1} = -\mathbf{v}^T \left(\sum_{i=2}^N \frac{1}{\lambda_i^2} u_i u_i^T \right) (L_1 - L_2) L \mathbf{v}, \\ \frac{d^2 H(k_1)}{dk_1^2} = 2\mathbf{v}^T \left(\sum_{i=2}^N \frac{1}{\lambda_i^3} u_i u_i^T \right) (L_1 - L_2)^2 L \mathbf{v}. \end{cases} \quad (15)$$

Equations (15) constitute the theoretical solution for H as a function of k_1 , being the λ_i the eigenvalues of the matrix $L_k = k_1(L_1 - L_2) + L_2$. By varying k_1 (for instance, increasing it), one can explore how the interplay of the spectra of $L_1 - L_2$ and L_2 might lead to non-trivial phenomena. Of particular interest, as noted before, is the set of parameters that optimize the system's stability. This can be represented as

$$\min H \text{ subject to } k_1 + k_2 = 1 \text{ with } 0 \leq k_1, k_2 < 1, \quad (16)$$

Similarly, the explicit solution of state change is

$$J = \int_0^\infty [T\delta\boldsymbol{\theta}(t)]^T [T\delta\boldsymbol{\theta}(t)] dt = \frac{1}{2} \mathbf{v}^T \left(\sum_{i=2}^N \frac{1}{\lambda_i} u_i u_i^T \right) \mathbf{v}. \quad (17)$$

With the matrices

$$Q_+ = [I_M \mid O_{M \times (N-M)}], \quad Q_- = [O_{(N-M) \times M} \mid I_{(N-M)}], \quad (18)$$

where I is the identity matrix and O is the zero matrix. The quantities J_+ and J_- can be expressed as

$$J_+ = \int_0^\infty \boldsymbol{\eta}_+^T(t) \boldsymbol{\eta}_+(t) dt = \int_0^\infty \delta\boldsymbol{\theta}^T(t) T^T Q_+^T Q_+ T \delta\boldsymbol{\theta}(t) dt, \quad (19)$$

$$J_- = \int_0^\infty \boldsymbol{\eta}_-^T(t) \boldsymbol{\eta}_-(t) dt = \int_0^\infty \delta\boldsymbol{\theta}^T(t) T^T Q_-^T Q_- T \delta\boldsymbol{\theta}(t) dt. \quad (20)$$

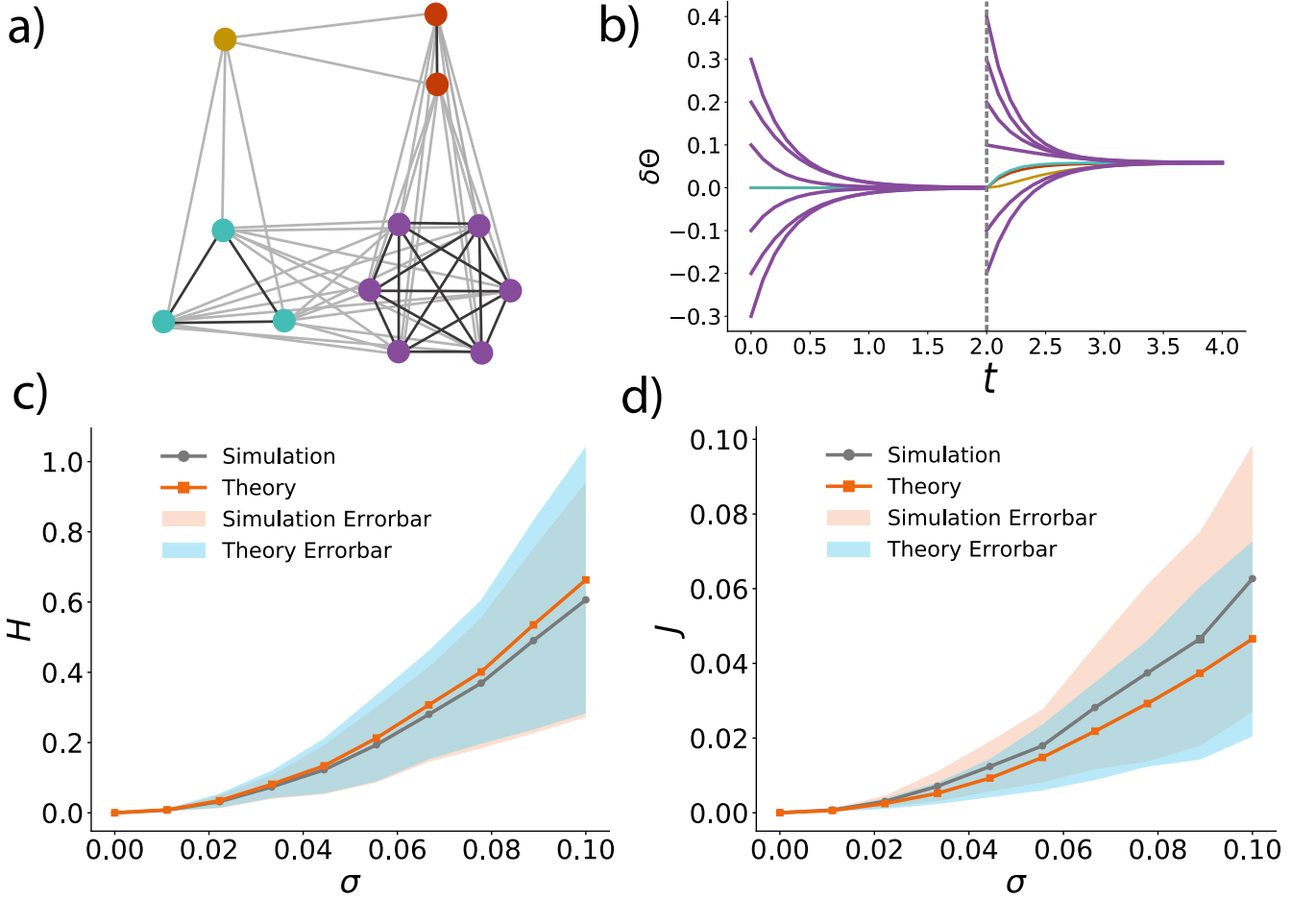


FIG. 1: Experimental observation of the model network. (a) The model network composed of 12 nodes with color representing cluster partition. (b) Disturbing the purple cluster subject to different conditions ($\sum_{i=7}^{12} v_i = 0$ at $t = 0$ and $\sum_{i=7}^{12} v_i \neq 0$ at $t = 2$) results in different steady states. (c) Variation between the numerical and the theoretical solutions of H with σ for the case of $k_1 = 0.9$ and $k_2 = 0.1$, where $\{v_i\}$ obey a normal distribution $N(0, \sigma)$. Each curve corresponds to the average over 100 realizations and the error bars represent the standard deviation. (d) Variation between the numerical and the theoretical solutions of J with σ in the same situation.

In order to check the accuracy of the proposed theoretical framework, we next use a toy network model composed of 12 nodes. Fig. 1(a) shows the topology of the network, with nodes of the same color belonging to the same cluster. The dark-color edges link nodes within each clusters while the light-color edges link nodes between clusters. If a perturbation of nodes is restricted to be within only one cluster, then we can use one unitary matrix T of the toy model and determine which clusters will be influenced (this depends on the nature of the perturbation). Fig. 1(b) illustrates the time series of each node (with color corresponding to different clusters) after two kinds of perturbations are applied as follows. At $t = 0$, we apply perturbations to nodes of the purple cluster with $\sum_{i=7}^{12} v_i = 0$; purple nodes are affected but other nodes remain unaffected. At $t = 2.0$, we again apply perturbations to purple nodes with $\sum_{i=7}^{12} v_i \neq 0$ and all nodes are affected. After application of the second perturbation, the system approaches a new synchronized state, and the coherency metric and state change quantify the state displacement during this process. Perturbations $\{v_i\}$ are in general assumed to obey a normal distribution $N(0, \sigma)$. The strength of perturbations or variations σ is crucial to the system stability. Fig. 1(c,d) illustrates the validation of numerical and theoretical solution of H and J with σ given, $k_1 = 0.9$ and $k_2 = 0.1$. With the increase of σ , the difference between the numerical and theoretical solution increases progressively as well as the standard deviation.

As noted before, the solutions Eqs. (15) might depend on the interplay/balance between L_1 and L_2 , which on its turn is determined by how k_1^* is changed. Here, we fix L_2 and proceed as follows to vary L_1 : i) we increase the connection strength by multiplying by an arbitrary coefficient ω , i.e., $L_k = k_1 \omega L_1 + k_2 L_2$, and ii) increase the connectivity of L_1 . Fig. 2(a) shows the coherency metric curve with respect to ω . When ω is relatively small, H increases monotonically with k_1 . However, when ω is relatively large, H first decreases and then increases with ω . In

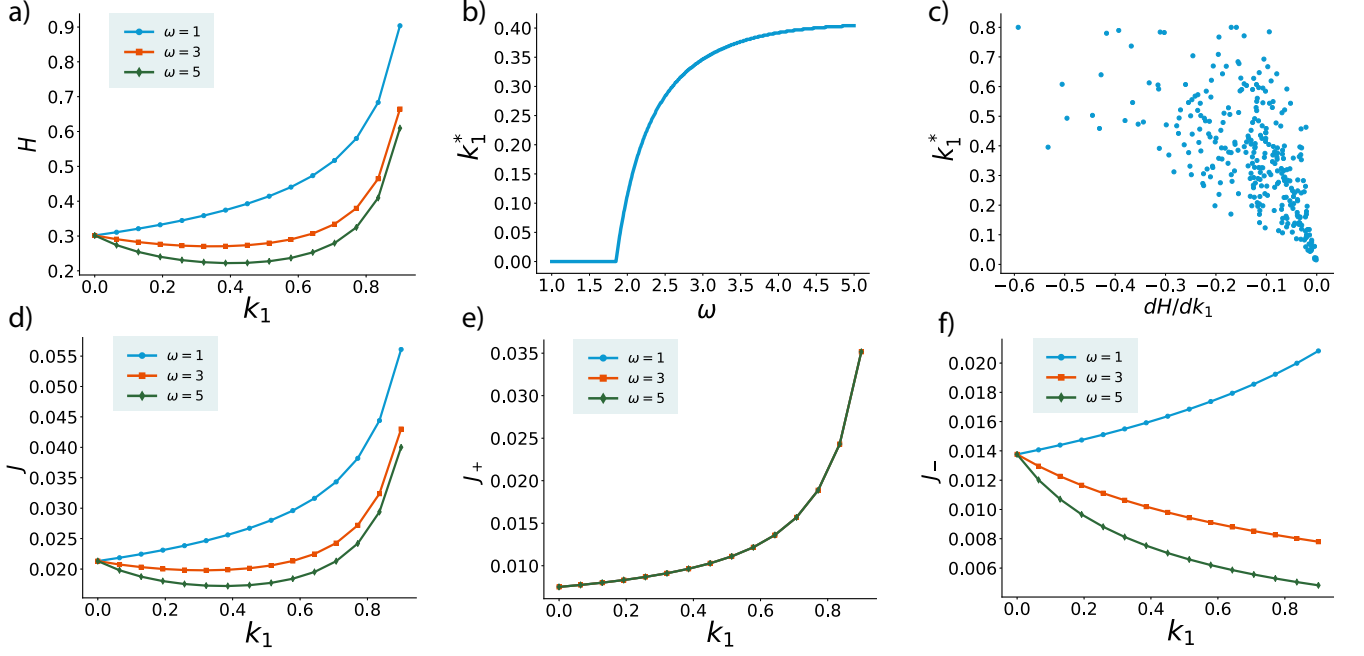


FIG. 2: Coherency metric and state change with $\omega = 1$, $\omega = 3$ and $\omega = 5$ for a given \mathbf{v} . (a) Coherency metric H with different ω . (b) Change of the minimum k_1^* with ω ranging from 1 to 5. (c) Relation between k_1^* and $\left. \frac{dH(k_1)}{dk_1} \right|_{k_1=\varepsilon}$ (set $\varepsilon = 0.01$) with $\omega = 5$ and $\{v_i\}$ obeying the normal distribution $N(0, 0.1)$ for 300 realizations. (d) State change J with different values of ω . (e) Intra-cluster state change J_+ with different ω s. (f) Inter-cluster state change J_- with different ω .

this case, H has one optimal solution located at k_1^* . Moreover, the value of k_1^* increases with ω , and the value of ω at which there is an optimal solution is larger than the critical point ω^* , see Fig. 2(b). Note that the critical value ω^* satisfies $0 = \left. \frac{\partial H(k_1, \omega)}{\partial k_1} \right|_{k_1=\varepsilon, \omega=\omega^*}$, where ε is close to 0.

Fig. 2(c) indicates that when $\left. \frac{dH(k_1)}{dk_1} \right|_{k_1=\varepsilon} < 0$, the smaller the slope of $H(\varepsilon)$, the closer k_1^* is to 0. We also calculate J when ω is varied. The explicit solutions of H and J , discussed above, indicate that there is only the difference of a constant in the Laplacian matrix between them. Thus, they share the same patterns, as illustrated in Fig. 2(d). The metric J corresponds to global properties of the whole system and consists of the intra-clusters integration across clusters J_+ and of the intra-clusters separation across clusters J_- . Further observation of J_+ and J_- reveals that the inter-cluster part is affected by different ω s, as illustrated in Fig. 2(e) and Fig. 2(f), due to the extra weight added to L_1 (the inter-cluster part of the Laplacian matrix). This also implies that the dynamics between and within clusters are, in a sense, separated.

In addition to the connection strength, we have also varied the connectivity of the network. Results are shown in Fig. 3. In particular, we find different coherency metric curves as well as state change curves with respect to different average degrees of the perturbed (purple) cluster. When the average degree is relatively small, both H and J increase monotonically with k_1 . However, when this average degree is relatively large (the fully connected network in Fig. 3(d)), H and J exhibit non-trivial solutions with a minimum at k_1^* . This situation is similar to that observed in Fig. 2 for high values of ω .

B. Dynamics of Mutualism networks

In addition to the Kuramoto model, we also consider another paradigmatic dynamics corresponding to a real system, e.g., that of mutualistic interactions among species in an ecological network. We consider the following equations [26] to describe the evolution of the number of individuals, or abundance, of species i , $x_i(t)$,

$$\dot{x}_i = B_i + r_i x_i \left(1 - \frac{x_i}{C_i} \right) \left(\frac{x_i}{G_i} - 1 \right) + \sum_{j=1}^N A_{ij} \frac{x_i x_j}{D_i + E_i x_i + H_j x_j}, \quad (21)$$

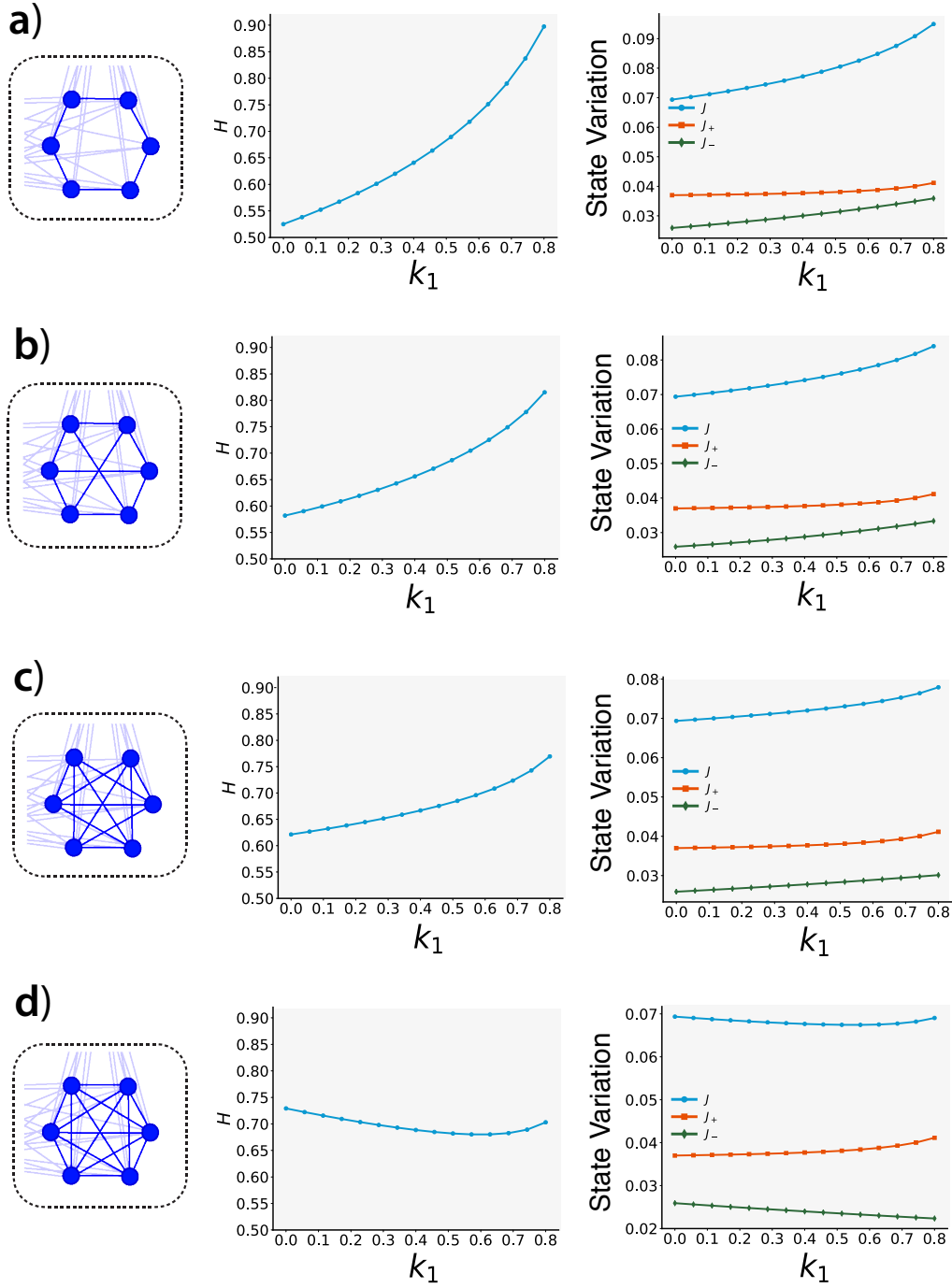


FIG. 3: Coherency metric and state change with different average inter-cluster degrees for the purple cluster in Figure 1 and for a given \mathbf{v} . (a) Average inter-cluster degree equals to 2. (b) Average inter-cluster degree equals to 3. (c) Average inter-cluster degree equals to 4. (d) Average inter-cluster degree equals to 5.

where, on the right hand side of the equation, the first term, B_i , captures the incoming migration rate of i from neighboring ecosystems; the second term accounts for the system's logistic growth with a carrying capacity C_i , and the Allee effect indicates that, for low population ($x_i < G_i < C_i$), the population size of species i decreases; the third term encodes the mutualistic dynamics, which is modulated by the mutualistic interactions (i, j) given by the matrix A . Here, we use symbiotic interactions A_{ij} constructed from plant-pollinator relationships as a classic kind of mutualistic relationships. Plants need pollinators to reproduce and pollinators feed mainly on nectar from plants.

In this system, the abundance x_i corresponds to one species i or cluster. Therefore, the second term quantifies the intra-species influence and the third term accounts for inter-species relations. Based on this system, we aim to quantify the balance of intra- and inter-cluster effects on the stability of the system. With this goal in mind, we additionally include the intra-species coupling strength k_1 in the second term of the above system of equations and the inter-species coupling strength k_2 to its third term. The additional coupling strengths k_1 and k_2 could account for exogenous factors with the capability of impacting the abundance of species in the system. For instance, favorable environmental conditions might create a better scenario in which pollinators and plants reproduce more. This would correspond to an increase of the intra-species coupling strength k_1 . We also note that the same conditions that favor the increase of k_1 might imply a reduction of k_2 . Thus, the final equations are

$$\dot{x}_i = B_i + k_1 r_i x_i \left(1 - \frac{x_i}{C_i}\right) \left(\frac{x_i}{G_i} - 1\right) + k_2 \sum_{j=1}^N A_{ij} \frac{x_i x_j}{D_i + E_i x_i + H_j x_j}. \quad (22)$$

We shall investigate the system stability by adjusting the balance between k_1 and k_2 . Here, following the above procedure, we have the constraint $k_1 + k_2 = 1$. Moreover, the underlying species interactions accounts for ecological interactions that are obtained from the web of life project. Specifically, each dataset is represented by a rectangular matrix M , with M_{ij} representing the mutualistic relationship between plant i and pollinator j . We construct the adjacency matrix A as

$$A = \begin{bmatrix} 0 & M \\ M^T & 0 \end{bmatrix}. \quad (23)$$

In other words, A represents interactions between different species (plants and pollinators) and competitive interactions between plants and pollinators are not given by the interaction matrix. However, if one projects links between the plants as the edges connected by pollinators, it is possible to define the pollinators' projection network. The (i, j) element of the corresponding adjacency matrix C_{po} equals 1 if pollinator i and pollinator j pollinate the same plant, or equals to 0 otherwise. Similarly, one can also define plants' projection links of the corresponding adjacency matrix C_{pl} . Altogether, the system of interactions can be considered as a two-layer network, whose sketch map is shown in Fig.4(a). The corresponding adjacency matrix is

$$\tilde{A} = \begin{bmatrix} C_{pl} & M \\ M^T & C_{po} \end{bmatrix}. \quad (24)$$

To investigate the balance with respect to intra- and inter-species coupling, we follow the above process. Specifically, we numerically integrate Eq. (22) and consider the following nonlinear programming problem

$$\min H \text{ subject to } k_1 + k_2 = 1 \text{ with } 0 \leq k_1, k_2 < 1. \quad (25)$$

The same process can also be followed for J . Note that here each node represents one species (cluster), and therein $J = J_+$ and $J_- = 0$.

There are 149 mutualistic networks provided by the web of life project. We have arbitrarily selected some of such networks for our numerical analysis. Results show that, depending on the selected networks, the coherency metric curves could either decrease first and then increase, or increase monotonically as shown in Fig. 5. The phenomena remain consistent for state change J . Fig. 5 shows these two limiting results obtained for two networks of the dataset (see S4 for more curves corresponding to different networks).

IV. CONCLUSIONS

Summarizing, in this manuscript we have investigated what is the impact that changes of the balance between intra- and inter-cluster coupling strengths induce on the stability of the system. In particular, we partition nodes into clusters using irreducible representation theory and linearize the system in the region of cluster synchronization. Depending on the nature of perturbations, only one or multiple clusters will be affected. We have proposed and evaluated two different metrics, namely H , which describes the energy that the system consumes to get back to a steady state, and J , which captures the state variations. The two metrics quantify stability, but from different points of view with respect to the coupling strength. Our results show that for both metrics the system could exhibit nontrivial behavior with variations of the intra- and inter-coupling strengths. The proposed theoretical approach has been applied to analyze two explicit dynamical models, e.g., the Kuramoto model and the dynamics of a mutualistic ecological network. For the first case, we have used a synthetic network, whereas the latter implements realistic systems. Our results could provide new hints in the quest to control the dynamics of networked systems.

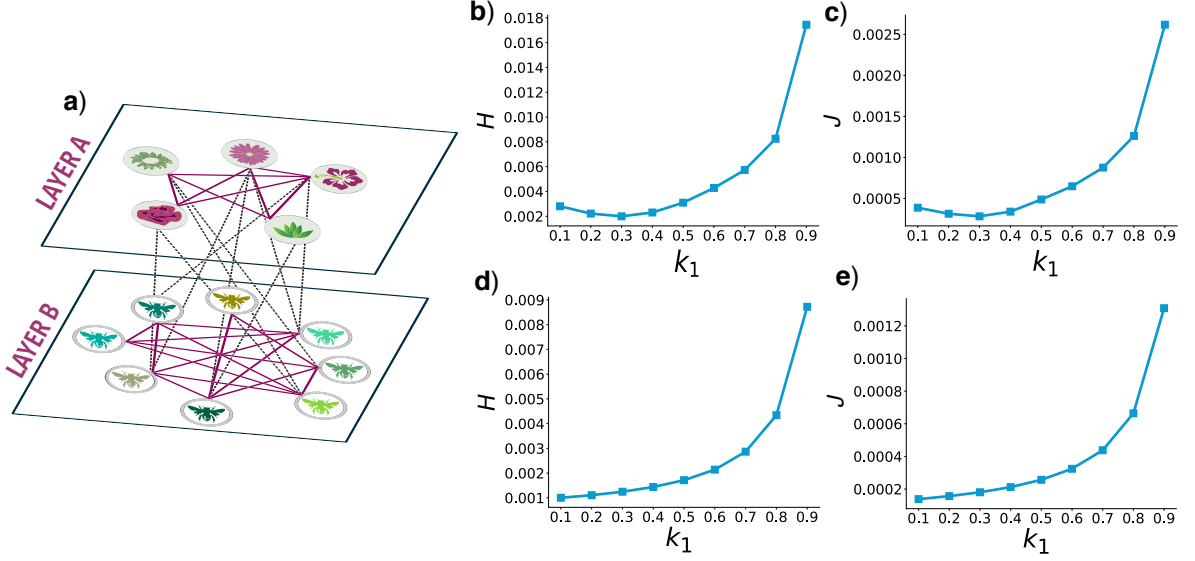


FIG. 4: The figure shows a schematic representation of a mutualistic network (panel a) and results for the coherency and state change metrics for two different mutualism networks (panels b through e). We have set $B_i = B = 0.01$, $r_i = r = 0.01$, $C_i = C = 5$, $G_i = G = 1$, $D_i = D = 5$, $E_i = E = 0.9$ and $H_i = H = 0.1$. \mathbf{v} obeys a normal distribution $N(0, 0.01)$. (b) Coherency metric for a network composed of 16 plants and 44 pollinators with 278 mutualistic interactions (network MPL46). (c) State change for the same network used in panel b. (d) Coherency metric for the network composed of 11 plants and 38 pollinators with 106 mutualistic interactions (network MPL08). (e) State change for the same network used in panel d.

Acknowledgement

This work has used the Web of Life dataset (www.web-of-life.es). PJ acknowledges National Key R&D Program of China (2018YFB0904500), Natural Science Foundation of Shanghai, the Program for Professor of Special Appointment (Eastern Scholar) at Shanghai Institutions of Higher Learning and by NSFC 269 (11701096), National Science Foundation of China under Grant 61773125. YM acknowledges partial support from Intesa Sanpaolo Innovation Center, the Government of Aragon, Spain through grant E36-17R (FENOL), and by MINECO and FEDER funds (FIS2017-87519-P).

Appendix: Details of mathematical derivations and further results.

S1. \mathbf{A} , \mathbf{T} and \mathbf{B} of the example

Using a discrete algebra software, it is straightforward to determine the symmetries of \mathbf{A} and the transformation matrix \mathbf{T} . We show the results applied to the network showed in Fig. 1(a):

$$A = \begin{bmatrix} 0 & 1 & 1 & 1 & 1 & 1 & 0 & 0 & 0 & 0 & 0 & 0 \\ 1 & 0 & 1 & 0 & 0 & 0 & 1 & 1 & 1 & 1 & 1 & 1 \\ 1 & 1 & 0 & 0 & 0 & 0 & 1 & 1 & 1 & 1 & 1 & 1 \\ 1 & 0 & 0 & 0 & 1 & 1 & 1 & 1 & 1 & 1 & 1 & 1 \\ 1 & 0 & 0 & 1 & 0 & 1 & 1 & 1 & 1 & 1 & 1 & 1 \\ 1 & 0 & 0 & 1 & 1 & 0 & 1 & 1 & 1 & 1 & 1 & 1 \\ 0 & 1 & 1 & 1 & 1 & 1 & 0 & 1 & 0 & 0 & 0 & 1 \\ 0 & 1 & 1 & 1 & 1 & 1 & 1 & 0 & 1 & 0 & 0 & 0 \\ 0 & 1 & 1 & 1 & 1 & 1 & 1 & 0 & 1 & 0 & 1 & 0 \\ 0 & 1 & 1 & 1 & 1 & 1 & 0 & 0 & 1 & 0 & 1 & 0 \\ 0 & 1 & 1 & 1 & 1 & 1 & 0 & 0 & 0 & 1 & 0 & 1 \\ 0 & 1 & 1 & 1 & 1 & 1 & 1 & 0 & 0 & 0 & 1 & 0 \end{bmatrix}. \quad (26)$$

There is one trivial cluster ($\{1\}$) and three non-trivial clusters ($\{2,3\}$, $\{4,5,6\}$ and $\{7,8,9,10,11,12\}$). The transformation matrix is

$$T = \begin{bmatrix} 0 & 0 & 0 & 0 & 0 & 0 & -\frac{\sqrt{6}}{6} & -\frac{\sqrt{6}}{6} & -\frac{\sqrt{6}}{6} & -\frac{\sqrt{6}}{6} & -\frac{\sqrt{6}}{6} & -\frac{\sqrt{6}}{6} \\ 1 & 0 & 0 & 0 & 0 & 0 & 0 & 0 & 0 & 0 & 0 & 0 \\ 0 & -\frac{\sqrt{2}}{2} & -\frac{\sqrt{2}}{2} & 0 & 0 & 0 & 0 & 0 & 0 & 0 & 0 & 0 \\ 0 & 0 & 0 & -\frac{\sqrt{3}}{3} & -\frac{\sqrt{3}}{3} & -\frac{\sqrt{3}}{3} & 0 & 0 & 0 & 0 & 0 & 0 \\ 0 & 0 & 0 & 0 & 0 & 0 & -\frac{\sqrt{6}}{6} & \frac{\sqrt{6}}{6} & -\frac{\sqrt{6}}{6} & \frac{\sqrt{6}}{6} & -\frac{\sqrt{6}}{6} & \frac{\sqrt{6}}{6} \\ 0 & -\frac{\sqrt{2}}{2} & \frac{\sqrt{2}}{2} & 0 & 0 & 0 & 0 & 0 & 0 & 0 & 0 & 0 \\ 0 & 0 & 0 & -\frac{\sqrt{6}}{3} & \frac{\sqrt{6}}{6} & \frac{\sqrt{6}}{6} & 0 & 0 & 0 & 0 & 0 & 0 \\ 0 & 0 & 0 & 0 & \frac{\sqrt{2}}{2} & -\frac{\sqrt{2}}{2} & 0 & 0 & 0 & 0 & 0 & 0 \\ 0 & 0 & 0 & 0 & 0 & 0 & 0 & -\frac{1}{2} & \frac{1}{2} & 0 & -\frac{1}{2} & \frac{1}{2} \\ 0 & 0 & 0 & 0 & 0 & 0 & -\frac{\sqrt{3}}{3} & \frac{\sqrt{3}}{6} & \frac{\sqrt{3}}{6} & -\frac{\sqrt{3}}{3} & \frac{\sqrt{3}}{6} & \frac{\sqrt{3}}{6} \\ 0 & 0 & 0 & 0 & 0 & 0 & 0 & -\frac{1}{2} & -\frac{1}{2} & 0 & \frac{1}{2} & \frac{1}{2} \\ 0 & 0 & 0 & 0 & 0 & 0 & -\frac{\sqrt{3}}{3} & -\frac{\sqrt{3}}{6} & \frac{\sqrt{3}}{6} & \frac{\sqrt{3}}{3} & \frac{\sqrt{3}}{6} & -\frac{\sqrt{3}}{6} \end{bmatrix}, \quad (27)$$

and the block diagonal coupling matrix is

$$B = \begin{bmatrix} 2 & 0 & 2\sqrt{3} & 3\sqrt{2} & 0 & 0 & 0 & 0 & 0 & 0 & 0 & 0 \\ 0 & 0 & -\sqrt{2} & -\sqrt{3} & 0 & 0 & 0 & 0 & 0 & 0 & 0 & 0 \\ 2\sqrt{3} & -\sqrt{2} & 1 & 0 & 0 & 0 & 0 & 0 & 0 & 0 & 0 & 0 \\ 3\sqrt{2} & -\sqrt{3} & 0 & 2 & 0 & 0 & 0 & 0 & 0 & 0 & 0 & 0 \\ 0 & 0 & 0 & 0 & -2 & 0 & 0 & 0 & 0 & 0 & 0 & 0 \\ 0 & 0 & 0 & 0 & 0 & -1 & 0 & 0 & 0 & 0 & 0 & 0 \\ 0 & 0 & 0 & 0 & 0 & 0 & -1 & 0 & 0 & 0 & 0 & 0 \\ 0 & 0 & 0 & 0 & 0 & 0 & 0 & -1 & 0 & 0 & 0 & 0 \\ 0 & 0 & 0 & 0 & 0 & 0 & 0 & 0 & -1 & 0 & 0 & 0 \\ 0 & 0 & 0 & 0 & 0 & 0 & 0 & 0 & 0 & -1 & 0 & 0 \\ 0 & 0 & 0 & 0 & 0 & 0 & 0 & 0 & 0 & 0 & 1 & 0 \\ 0 & 0 & 0 & 0 & 0 & 0 & 0 & 0 & 0 & 0 & 0 & 1 \end{bmatrix}. \quad (28)$$

S2. Detailed proof of the explicit solution of \mathbf{H} and its derivative

The key point of the equality in Equation (14) and Equation (15) lies in whether L_1 commutes with L_2 . The Laplacian matrix of the network is

$$L = \begin{bmatrix} 5 & -1 & -1 & -1 & -1 & -1 & 0 & 0 & 0 & 0 & 0 & 0 \\ -1 & 8 & -1 & 0 & 0 & 0 & -1 & -1 & -1 & -1 & -1 & -1 \\ -1 & -1 & 8 & 0 & 0 & 0 & -1 & -1 & -1 & -1 & -1 & -1 \\ -1 & 0 & 0 & 9 & -1 & -1 & -1 & -1 & -1 & -1 & -1 & -1 \\ -1 & 0 & 0 & -1 & 9 & -1 & -1 & -1 & -1 & -1 & -1 & -1 \\ -1 & 0 & 0 & -1 & -1 & 9 & -1 & -1 & -1 & -1 & -1 & -1 \\ 0 & -1 & -1 & -1 & -1 & -1 & 7 & -1 & 0 & 0 & 0 & -1 \\ 0 & -1 & -1 & -1 & -1 & -1 & -1 & 7 & -1 & 0 & 0 & 0 \\ 0 & -1 & -1 & -1 & -1 & -1 & 0 & -1 & 7 & -1 & 0 & 0 \\ 0 & -1 & -1 & -1 & -1 & -1 & 0 & 0 & -1 & 7 & -1 & 0 \\ 0 & -1 & -1 & -1 & -1 & -1 & 0 & 0 & 0 & -1 & 7 & -1 \\ 0 & -1 & -1 & -1 & -1 & -1 & -1 & 0 & 0 & 0 & -1 & 7 \end{bmatrix}. \quad (29)$$

The intra-cluster part is

$$L_1 = \begin{bmatrix} 0 & 0 & 0 & 0 & 0 & 0 & 0 & 0 & 0 & 0 & 0 & 0 \\ 0 & 1 & -1 & 0 & 0 & 0 & 0 & 0 & 0 & 0 & 0 & 0 \\ 0 & -1 & 1 & 0 & 0 & 0 & 0 & 0 & 0 & 0 & 0 & 0 \\ 0 & 0 & 0 & 2 & -1 & -1 & 0 & 0 & 0 & 0 & 0 & 0 \\ 0 & 0 & 0 & -1 & 2 & -1 & 0 & 0 & 0 & 0 & 0 & 0 \\ 0 & 0 & 0 & -1 & -1 & 2 & 0 & 0 & 0 & 0 & 0 & 0 \\ 0 & 0 & 0 & 0 & 0 & 0 & 2 & -1 & 0 & 0 & 0 & -1 \\ 0 & 0 & 0 & 0 & 0 & 0 & -1 & 2 & -1 & 0 & 0 & 0 \\ 0 & 0 & 0 & 0 & 0 & 0 & 0 & -1 & 2 & -1 & 0 & 0 \\ 0 & 0 & 0 & 0 & 0 & 0 & 0 & 0 & -1 & 2 & -1 & 0 \\ 0 & 0 & 0 & 0 & 0 & 0 & 0 & 0 & 0 & -1 & 2 & -1 \\ 0 & 0 & 0 & 0 & 0 & 0 & -1 & 0 & 0 & 0 & -1 & 2 \end{bmatrix}, \quad (30)$$

and the inter-cluster part is

$$L_2 = \begin{bmatrix} 5 & -1 & -1 & -1 & -1 & -1 & 0 & 0 & 0 & 0 & 0 & 0 \\ -1 & 7 & 0 & 0 & 0 & 0 & -1 & -1 & -1 & -1 & -1 & -1 \\ -1 & 0 & 7 & 0 & 0 & 0 & -1 & -1 & -1 & -1 & -1 & -1 \\ -1 & 0 & 0 & 7 & 0 & 0 & -1 & -1 & -1 & -1 & -1 & -1 \\ -1 & 0 & 0 & 0 & 7 & 0 & -1 & -1 & -1 & -1 & -1 & -1 \\ -1 & 0 & 0 & 0 & 0 & 7 & -1 & -1 & -1 & -1 & -1 & -1 \\ 0 & -1 & -1 & -1 & -1 & -1 & 5 & 0 & 0 & 0 & 0 & 0 \\ 0 & -1 & -1 & -1 & -1 & -1 & 0 & 5 & 0 & 0 & 0 & 0 \\ 0 & -1 & -1 & -1 & -1 & -1 & 0 & 0 & 5 & 0 & 0 & 0 \\ 0 & -1 & -1 & -1 & -1 & -1 & 0 & 0 & 0 & 5 & 0 & 0 \\ 0 & -1 & -1 & -1 & -1 & -1 & 0 & 0 & 0 & 0 & 5 & 0 \\ 0 & -1 & -1 & -1 & -1 & -1 & 0 & 0 & 0 & 0 & 0 & 5 \end{bmatrix}. \quad (31)$$

Since two symmetric matrices are commutative if and only if their matrix product is symmetric, we just need to prove that $L_1 L_2$ is symmetric. In other words, if we let $L_1 = [\ell_1^{(1)}, \ell_2^{(1)}, \dots, \ell_N^{(1)}]$ and $L_2 = [\ell_1^{(2)}, \ell_2^{(2)}, \dots, \ell_N^{(2)}]$, we need to prove $\ell_i^{(1)T} \ell_j^{(2)} = \ell_j^{(1)T} \ell_i^{(2)}$ for any $1 \leq i, j \leq N$. Consider the following two situations:

- i) Node i and node j belong to different clusters. We set cluster $C_{\alpha(i)} = [i_1, i_2, \dots, i_{N_{\alpha(i)}}]$. Because of the definition of L_1 , only the i_1 th, i_2 th, \dots , $i_{N_{\alpha(i)}}$ th components of $\ell_i^{(1)}$ have nonzero values and their sum equals 0. The corresponding components of $\ell_j^{(2)}$ all equal to -1 if cluster $C_{\alpha(i)}$ and cluster $C_{\alpha(j)}$ are connected, or 0 otherwise. No matter whether cluster $C_{\alpha(i)}$ and cluster $C_{\alpha(j)}$ are connected, $\ell_i^{(1)T} \ell_j^{(2)} = 0$. Similarly, we get $\ell_j^{(1)T} \ell_i^{(2)} = 0$ and $\ell_i^{(1)T} \ell_j^{(2)} = \ell_j^{(1)T} \ell_i^{(2)}$.
- ii) Node i and node j belong to the same cluster. As mentioned in i), only the i_1 th, i_2 th, \dots , $i_{N_{\alpha(i)}}$ th components of $\ell_i^{(1)}$ have nonzero values. The corresponding components of $\ell_j^{(2)}$ are equal to $d_j^{(2)}$ if they are diagonal elements of L , or 0 otherwise. $\ell_i^{(1)T} \ell_j^{(2)}$ equals to $-d_j^{(2)}$ if node i and node j are connected, or 0 otherwise. Similarly, we get the same case of $\ell_j^{(1)T} \ell_i^{(2)}$ and $\ell_i^{(1)T} \ell_j^{(2)} = \ell_j^{(1)T} \ell_i^{(2)}$.

To sum up, L_1 and L_2 are commutative. L and L_k are the linear combination of L_1 and L_2 so that every pair of these four matrices is commutative. Next, we prove Equation (14) and Equation (15). Substituting Equation (13) into Equation (4), we obtain

$$H = 2 \int_0^\infty \delta \theta^T L \delta \theta dt = 2 \int_0^\infty \mathbf{v}^T e^{-L_k t} L e^{-L_k t} \mathbf{v} dt. \quad (32)$$

The expansion of $e^{-L_k t}$ in matrix power series reads

$$e^{-L_k t} = \sum_{n=0}^{\infty} \frac{1}{n!} (-L_k t)^n = \sum_{n=0}^{\infty} \frac{(-t)^n}{n!} (k_1 L_1 + k_2 L_2)^n = \sum_{n=0}^{\infty} \frac{(-t)^n}{n!} \sum_{m=0}^n (k_1 L_1)^m (k_2 L_2)^{n-m}, \quad (33)$$

and $e^{-L_k t}$ commutes with L . This gives

$$H = 2\mathbf{v}^T \int_0^\infty e^{-2L_k t} dt L\mathbf{v}. \quad (34)$$

According to the theory of spectral decomposition, $e^{-2L_k t} = \sum_{i=2}^N e^{-2\lambda_i t} u_i u_i^T$, where λ_i and u_i ($i = 2, 3, \dots, N$) are the eigenvalues of L_k from the smallest to the largest (except for $\lambda_1 = 0$) and u_i their corresponding eigenvectors. Furthermore, as L_k is positive semidefinite, all eigenvalues of L_k are non-negative. Actually, except for $\lambda_1 = 0$, the rest of eigenvalues are all positive so that the integral $\int_0^\infty e^{-2\lambda_i t} dt$ is convergent. These conclusions combined lead to

$$H = 2\mathbf{v}^T \int_0^\infty \sum_{i=2}^N e^{-2\lambda_i t} u_i u_i^T dt L\mathbf{v} = 2\mathbf{v}^T \sum_{i=2}^N \int_0^\infty e^{-2\lambda_i t} dt u_i u_i^T L\mathbf{v} = \mathbf{v}^T \left(\sum_{i=2}^N \frac{1}{\lambda_i} u_i u_i^T \right) L\mathbf{v}. \quad (35)$$

Similarly, the first derivative of H is

$$\frac{dH(k_1)}{dk_1} = 2\mathbf{v}^T \int_0^\infty \frac{d}{dk_1} (e^{-2[k_1(L_1-L_2)+L_2]t}) dt L\mathbf{v} = -\mathbf{v}^T \left(\sum_{i=2}^N \frac{1}{\lambda_i^2} u_i u_i^T \right) (L_1 - L_2) L\mathbf{v}, \quad (36)$$

and the second derivative of H is

$$\frac{d^2 H(k_1)}{dk_1^2} = -4\mathbf{v}^T \int_0^\infty \frac{d}{dk_1} (e^{-2L_k t}) t dt (L_1 - L_2) L\mathbf{v} = 2\mathbf{v}^T \left(\sum_{i=2}^N \frac{1}{\lambda_i^3} u_i u_i^T \right) (L_1 - L_2)^2 L\mathbf{v}. \quad (37)$$

S3. Further explanation of the choice of \mathbf{v} .

The choice of v has a direct effect on whether H has the minimum value in $(0,1)$. The key point lies in the sign of $\left. \frac{dH(k_1)}{dk_1} \right|_{k_1=\varepsilon}$.

Let $Q = \sum_{i=2}^N \frac{1}{\lambda_i^2} u_i u_i^T (L_1 - L_2) L$. Q is symmetric so that its eigenvectors compose an orthogonal basis. Denote its eigenvalues and eigenvectors by $\{\mu_i\}_{i=1}^N$ and $\{q_i\}_{i=1}^N$. \mathbf{v} can be rewritten as the linear combination of $\{q_i\}_{i=1}^N$, i.e., $\mathbf{v} = \sum_i \beta_i q_i$. $\frac{dH(k_1)}{dk_1}$ can be expressed as:

$$\frac{dH(k_1)}{dk_1} = -\mathbf{v}^T Q \mathbf{v} = -\left(\sum_i \beta_i q_i^T \right) Q \left(\sum_j \beta_j q_j \right) = -\sum_{i,j} \beta_i \beta_j q_i^T Q q_j = -\sum_{i,j} \mu_j \beta_i \beta_j q_i^T q_j = -\sum_i \mu_i \beta_i^2. \quad (38)$$

That is, for the given $k_1 = \varepsilon$, we can distribute $\{\beta_i\}$ to ensure that Equation (38) is less than 0 and H has the minimum point in $(0,1)$.

S4. More curves corresponding to different mutualism networks

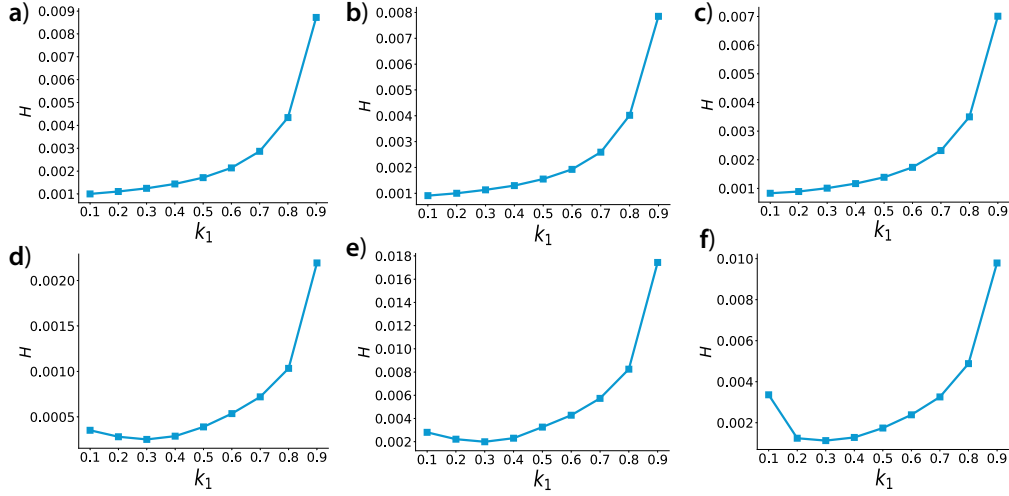


FIG. 5: Coherency metric curve corresponding to six different mutualism networks. We set $B_i = B = 0.01$, $r_i = r = 0.01$, $C_i = C = 5$, $G_i = G = 1$, $D_i = D = 5$, $E_i = E = 0.9$ and $H_i = H = 0.1$. \mathbf{v} obeys a normal distribution $N(0, 0.01)$. (a) 11 plants and 38 pollinators with 106 mutualistic interactions (network MPL08). (b) 14 plants and 13 pollinators with 52 mutualistic interactions (network MPL11). (c) 7 plants and 33 pollinators with 65 mutualistic interactions (network MPL32). (d) 10 plants and 12 pollinators with 30 mutualistic interactions (network MPL36). (e) 16 plants and 44 pollinators with 278 mutualistic interactions (network MPL46). (f) 14 plants and 35 pollinators with 86 mutualistic interactions (network MPL50).

Fig. 5 shows the coherency metric curve corresponding to six different mutualism networks. State change curves have similar patterns, which are omitted here. The result indicates that both patterns of coherency metric and state change are common in nature.

-
- [1] Steven H Strogatz. Exploring complex networks. *Nature*, 410(6825):268–276, 2001.
 - [2] Mark Ed Newman, Albert-László Ed Barabási, and Duncan J Watts. *The structure and dynamics of networks*. Princeton university press, 2006.
 - [3] Stefano Boccaletti, Vito Latora, Yamir Moreno, Martin Chavez, and D-U Hwang. Complex networks: Structure and dynamics. *Physics Reports*, 424(4-5):175–308, 2006.
 - [4] Francisco A Rodrigues, Thomas K DM Peron, Peng Ji, and Jürgen Kurths. The kuramoto model in complex networks. *Physics Reports*, 610:1–98, 2016.
 - [5] S Boccaletti, JA Almendral, S Guan, I Leyva, Z Liu, I Sendiña-Nadal, Z Wang, and Y Zou. Explosive transitions in complex networks—structure and dynamics: Percolation and synchronization. *Physics Reports*, 660:1–94, 2016.
 - [6] Francesco Sorrentino, Louis M Pecora, Aaron M Hagerstrom, Thomas E Murphy, and Rajarshi Roy. Complete characterization of the stability of cluster synchronization in complex dynamical networks. *Science Advances*, 2(4):e1501737, 2016.
 - [7] Tommaso Menara, Giacomo Baggio, Danielle Bassett, and Fabio Pasqualetti. Stability conditions for cluster synchronization in networks of heterogeneous kuramoto oscillators. *IEEE Transactions on Control of Network Systems*, 7(1):302–314, 2019.
 - [8] Young Sul Cho, Takashi Nishikawa, and Adilson E Motter. Stable chimeras and independently synchronizable clusters. *Physical Review Letters*, 119(8):084101, 2017.
 - [9] Louis M Pecora, Francesco Sorrentino, Aaron M Hagerstrom, Thomas E Murphy, and Rajarshi Roy. Cluster synchronization and isolated desynchronization in complex networks with symmetries. *Nature Communications*, 5(1):1–8, 2014.
 - [10] Ed Bullmore and Olaf Sporns. Complex brain networks: graph theoretical analysis of structural and functional systems. *Nature Reviews Neuroscience*, 10(3):186–198, 2009.
 - [11] Olaf Sporns. Structure and function of complex brain networks. *Dialogues in Clinical Neuroscience*, 15(3):247–262, 2013.
 - [12] Changsong Zhou, Lucia Zemanová, Gorka Zamora, Claus C Hilgetag, and Jürgen Kurths. Hierarchical organization unveiled by functional connectivity in complex brain networks. *Physical Review Letters*, 97(23):238103, 2006.
 - [13] Jason Z Kim, Jonathan M Soffer, Ari E Kahn, Jean M Vettel, Fabio Pasqualetti, and Danielle S Bassett. Role of graph architecture in controlling dynamical networks with applications to neural systems. *Nature Physics*, 14(1):91–98, 2018.

- [14] Martin Rohden, Andreas Sorge, Marc Timme, and Dirk Witthaut. Self-organized synchronization in decentralized power grids. *Physical Review Letters*, 109(6):064101, 2012.
- [15] Florian Dörfler and Francesco Bullo. Synchronization in complex networks of phase oscillators: A survey. *Automatica*, 50(6):1539–1564, 2014.
- [16] Peter J Menck, Jobst Heitzig, Jürgen Kurths, and Hans Joachim Schellnhuber. How dead ends undermine power grid stability. *Nature Communications*, 5(1):1–8, 2014.
- [17] Yang Yang and Adilson E Motter. Cascading failures as continuous phase-space transitions. *Physical Review Letters*, 119(24):248302, 2017.
- [18] Liyue Zhang, Adilson E Motter, and Takashi Nishikawa. Incoherence-mediated remote synchronization. *Physical Review Letters*, 118(17):174102, 2017.
- [19] Andrew J Whalen, Sean N Brennan, Timothy D Sauer, and Steven J Schiff. Observability and controllability of nonlinear networks: The role of symmetry. *Physical Review X*, 5(1):011005, 2015.
- [20] Vincenzo Nicosia, Miguel Valencia, Mario Chavez, Albert Díaz-Guilera, and Vito Latora. Remote synchronization reveals network symmetries and functional modules. *Physical Review Letters*, 110(17):174102, 2013.
- [21] Martin Golubitsky, Ian Stewart, and David G Schaeffer. *Singularities and groups in bifurcation theory*, volume 2. Springer Science & Business Media, 2012.
- [22] Chenbo Fu, Zhigang Deng, Liang Huang, and Xingang Wang. Topological control of synchronous patterns in systems of networked chaotic oscillators. *Physical Review E*, 87(3):032909, 2013.
- [23] Caitlin RS Williams, Thomas E Murphy, Rajarshi Roy, Francesco Sorrentino, Thomas Dahms, and Eckehard Schöll. Experimental observations of group synchrony in a system of chaotic optoelectronic oscillators. *Physical Review Letters*, 110(6):064104, 2013.
- [24] Chittaranjan Hens, Uzi Harush, Simi Haber, Reuven Cohen, and Baruch Barzel. Spatiotemporal signal propagation in complex networks. *Nature Physics*, 15(4):403–412, 2019.
- [25] Saverio Bolognani, Bala K Poolla, and Florian Dörfler. Optimal placement of virtual inertia in power grids. *Automatic Control, IEEE Transactions on*, 62(12):6209–6220, 2017.
- [26] Jianxi Gao, Baruch Barzel, and Albert-László Barabási. Universal resilience patterns in complex networks. *Nature*, 530(7590):307–312, 2016.